https://doi.org/10.1016/j.engstruct.2019.01.069

Structural behavior of cold-formed steel semi-oval hollow section beams

Man-Tai Chen [a,*], Ben Young [b]

[a] *Department of Civil Engineering, The University of Hong Kong, Pokfulam Road, Hong Kong, China.*

[b] *Department of Civil and Environmental Engineering, The Hong Kong Polytechnic University, Hong Kong, China. (Formerly, Department of Civil Engineering, The University of Hong Kong, Pokfulam Road, Hong Kong, China)*

Abstract

The structural behavior of cold-formed steel semi-oval hollow sections under bending was studied through experimental and numerical investigation. The semi-oval hollow sections investigated in this study were cold-formed from hot-extruded seamless carbon steel circular hollow sections. A total of 20 beams was tested for both four-point and three-point bending configurations. The sections were bent about the major axis in both positive and negative directions. The tests were replicated numerically by means of rigorous finite element analyses. Based on the validated finite element model, an extensive parametric study was conducted on 198 beam specimens with a wide range of cross-section geometries subjected to pure bending about the major axis in both positive and negative directions. The current design rules for steel structures, such as Australian/New Zealand standards, European codes as well as American and the North American specifications, do not cover the design of semi-oval hollow sections. Therefore, the ultimate flexural capacities of beam specimens obtained from the test program and numerical investigation were only compared with the design strengths predicted by the Direct Strength Method and the Continuous Strength Method. The applicability and reliability of these two design methods were evaluated through reliability analysis. The results show that the existing design methods provide quite conservative and scattered design strength predictions for cold-formed steel semi-oval hollow section beams. In this study, modifications on the Direct Strength Method and the Continuous Strength Method are proposed, which provide better design strength predictions with improved accuracy in a reliable manner.

Keywords: Beams; Cold-formed steel; Finite element model; Semi-oval hollow sections; Structural design.

---

* Corresponding author.
E-mail address: cmt111@connect.hku.hk (M.T. Chen).

1. Introduction

Traditionally, the family of tubular sections comprises rectangular, square and circular hollow sections. The square and circular sections with equal geometric properties in two principle axes are often used in the compression member to resist the predominant axial load [1, 2], while the rectangular section with different structural attributes in major and minor axes is often designed to carry the bending moment. Owing to the development of cold-forming technology, tubular sections with different desirable cross-section profile can be easily fabricated [3-6]. The semi-oval hollow section (SOHS) with three flat faces and one semi-circular face has recently emerged in the market. With the possession of different major and minor axes properties, the SOHS can be oriented to resist the bending moment effectively without jeopardizing the architectural appearance by exposing the semi-circular face. Nevertheless, even though the SOHS has prominent advantages in both structural and aesthetical aspects, there is a lack of investigation and design information available for this newly developed section type [7-9].

This paper presents the experimental and numerical investigation on the structural behavior of cold-formed steel semi-oval hollow section beams. The test program consisted of 20 beam tests conducted in four-point and three-point bending configurations with the beam specimens bent about the major axis in both positive and negative directions. Finite element (FE) models were developed and validated against the test results. An extensive parametric study was performed on SOHS under pure bending with a wide range of cross-section geometries. The current design specifications for steel structures [10-13] do not cover the structural design of cold-formed steel SOHS. Supplementing the experimental results with the results obtained from parametric study, the test and FE strengths were only compared with the design strengths predicted by the Direct Strength Method (DSM) [11] and the Continuous Strength Method (CSM) [14-16]. Modifications on Direct Strength Method and Continuous Strength Method are proposed in this study. The applicability and reliability of the existing and modified Direct Strength Methods and Continuous Strength Methods were evaluated through reliability analysis.

2. Experimental investigation

2.1. Test specimens

Four-point and three-point bending tests were conducted on cold-formed steel semi-oval hollow sections. A total of 20 beam specimens was tested in this study. The cold-formed steel SOHS were bent about the major axis in both positive direction (Curved flange in compression) and negative direction (Flat flange in compression). Four series of SOHS with different cross-sectional geometric properties were included in the experimental program. The cross-section geometry of SOHS is defined with the symbols as shown in Fig. 1. The nominal dimensions ($D\times B\times t$) of SOHS are 93×62×5.5, 107×68×6.5, 108×79×5.5 and 125×85×6.5, where D, B and t are the overall depth, overall width and thickness of the sections, respectively. The nominal cross-section aspect ratio (D/B) of the specimens varied slightly from 1.37 to 1.57. The test specimens were fabricated by hot-extruded seamless steel circular hollow sections and then cold-formed into SOHS. Therefore, the SOHS are considered as cold-formed steel sections due to the involvement of the final cold-forming process.

The specimens are labeled in a way that the nominal cross-section geometry, bending configuration and bending direction can be identified. The specimen label consists of two parts, which are separated by a hyphen. The first part of the label identifies the nominal cross-section geometry of the test specimen. The second part reveals the bending configuration and the bending direction of the specimen. The number following a hyphen indicates the bending configuration of specimen, where the number “3” and “4” mean three-point and four-point bending configurations, respectively. The following letter designates the bending direction of specimen, where “C” and “F” indicate beam specimen subjected to bending about the major axis in positive (Curved flange in compression) and negative (Flat flange in compression) directions, respectively. If a test is repeated, then a symbol of “#” is added in the label. For example, the label 108×79×5.5-3F# represents a repeated test of a specimen subjected to bending about the major axis in negative direction for three-point bending configuration with nominal cross-sectional dimensions of overall depth (D), overall width (B) and thickness (t) equal to 108, 79 and 5.5 mm, respectively. The measured specimen

dimensions are reported in Table 1, where r_o and r_i are the external and internal corner radii, respectively, and L is the total specimen length.

2.2. Material properties

Tensile coupon tests were conducted to determine the material properties of the test specimens and to investigate the strength enhancement due to the cold-forming process. Tensile coupon specimens were extracted from the same batch of specimens as used in the bending tests and were machined longitudinally along the flat web (TC1), the semi-circular flange (TC2) and the corner (TC3) of SOHS as shown in Fig. 2. The static material properties of the coupon specimens at three different locations were obtained and are reported by Chen and Young [7] as summarized in Table 2, where E is the Young's modulus, $\sigma_{0.2}$ is the 0.2% tensile proof stress, σ_u is the ultimate tensile strength and ε_f is the tensile strain at fracture.

2.3. Test setup and procedure

The beam specimens were subjected to bending about the major axis in both positive and negative directions. Other than determining the moment capacities and failure modes of beam specimens, the moment-curvature relationship of specimens under constant moment and the moment-rotation relationship of specimens under a moment gradient were also investigated through four-point and three-point bending tests, respectively.

Ten four-point bending tests, five bending about the major axis in positive direction and five in negative direction, were conducted to obtain the moment capacities and the moment-curvature relationships of specimens under constant moment. The schematic illustration of the test setup and a view of experimental arrangement of four-point bending test are shown in Fig. 3. The beams were simply supported by two rollers at the ends and loaded through one half-round and one roller located at the loading points. In four-point bending configuration, the moment span between the two loading points (L_m = 600 mm) and the shear spans between the end supports and the adjacent loading points (L_s = 580 mm) were carefully designed so that no occurrence of shear failure was observed. The total

specimen length of all beam specimens subjected to four-point bending was 1900 mm as shown in Table 1. The semi-circular flange of specimen was seated on the customized made steel sitting mounted on the load transfer plate and the flat flange of specimen was seated on the load transfer plate directly in order to provide uniform distributed loads at the supports and loading points. In addition, stiffening plates clamped to the webs, wooden blocks inserted inside the specimens at the loading locations together with the steel sittings were installed to prevent any possible web crippling and local bearing failure during testing. Three 100 mm linear variable displacement transducers (LVDTs) were placed beneath the specimen at the locations of the two loading points and mid-span of the specimen to capture the real-time vertical deflections. Hence, the curvature of each specimen was also obtained. Displacement controlled loading method was employed to drive the hydraulic actuator at a constant speed of 2 mm/min for all beam tests. The applied displacement was paused for 100 seconds at the ultimate load to allow for stress relaxation and to obtain the static load. Therefore, static moment capacities were obtained. A data requisition system was used to record the applied load and the readings of the LVDTs at one second interval during the tests.

Ten three-point bending tests, five bending about the major axis in positive direction and five in negative direction, were conducted for the purpose of assessing the moment capacities and the moment-rotation relationships of specimens under a moment gradient. The schematic and test setups of three-point bending test are shown in Fig. 4. Similar to four-point bending, simply supported boundary condition was also simulated by two roller supports. The beams were loaded through a half-round support. In three-point bending configuration, the total span of beam specimen was taken as twice of the shear span (L_s) of beam specimen, which had the same shear span as the four-point bending counterpart. The total specimen length of all beam specimens subjected to three-point bending was 1300 mm as shown in Table 1. Two 25 mm LVDTs were installed at each support of specimen to measure the end rotation, whilst one 100 mm LVDT was placed at the mid-span to measure the vertical displacement of the specimens. The three-point bending tests used the same test rig, loading method and data acquisition as the four-point bending tests.

2.4. Test results

No shear failure and out-of-plane bending were observed in all beam tests. For beam specimens under four-point bending, all specimens failed within the moment span. The static moment-curvature relationships for specimens subjected to bending about the major axis in positive and negative directions were derived and are depicted in Fig. 5(a) and (b), respectively. For three point-bending tests, all beam specimens failed near mid-span. The static moment-rotation curves for specimens subjected to bending about the major axis in positive and negative directions are plotted in Fig. 6(a) and (b), respectively. Photos of failed specimens are shown in Fig. 7. From the experimental results, it is found that all beam specimens failed in flexural buckling, since the semi-oval hollow sections investigated in this study were compact. The experimental moment capacities of SOHS beam specimens under a moment gradient ($M_{Exp,3}$) and constant moment ($M_{Exp,4}$) are summarized in Table 3. It is found that the results of repeated tests are very close to their corresponding first test values. Therefore, the reliability of the test results was demonstrated by the small differences between the repeated test values and their corresponding first test values. It is worth noting that for the same cross-section, specimens under a moment gradient reached a higher moment capacity than their counterparts that were subjected to constant moment by 11% on average. The reason for this phenomenon is illustrated as follows. When the specimen in three-point bending configuration reached the plastic moment at mid-span in the loading point, the adjacent portions, which were at lower stress level, provided restraint to the mostly stressed region and helped to delay inelastic local buckling, whilst in four-point bending, the whole central region (moment span) experienced constant moment and stress level, hence no stabilizing effect is provided to the moment span. In addition, only when a plastic hinge with certain length is formed will lead to the drop of load and failure of specimen. By that time, the bending moment experienced at the mid span in three-point bending already reached a higher value.

3. Finite element models

The finite element models using the program ABAQUS of version 6.14 were established to simulate the beam tests conducted on cold-formed steel SOHS. In the validation of finite element

models, the measured cross-section geometries as reported in Table 1, the measured Young's modulus and the converted true plastic stress-strain response were used. Full length of beam specimens was modeled. To replicate the four-point and three-point bending test configurations, the roller supports and half-round support with the customized made steel sittings and stiffening plates were simulated by coupling the displacements of the stiffened regions at the supports and loading points to the displacements of the corresponding reference points located a certain distance away from the tip of contacting points of specimens at the cross-section centerline. All out-of-plane displacements of the reference points and the translation of the reference point related to the half-round support were restrained.

The S4R shell element with four nodes and reduced integration (S4R) was selected for beam members. The value of $(B+D)/30$ was taken as the mesh size in the flat and semi-circular portions, whilst finer mesh was used for corner region. The mesh was assigned uniformly in longitudinal direction of the beam models.

Bending and membrane residual stresses were introduced to the section during the cold-forming process. The magnitude of membrane residual stress and its corresponding effect upon structural performance of steel members are much less than those of the bending residual stress [17-20]. Since the bending residual stress with larger magnitude and more significant effect has already been included into the measured material properties [7], it is rational not to explicitly incorporate the residual stresses into the finite element models [21-24]. To further verify the unnecessity of explicit inclusion of residual stress, the measured membrane residual stress distribution for SOHS with nominal dimensions of 125×85×6.5 was incorporated explicitly in the FE model by dividing the cross-section into strips and assigning the membrane residual stresses to each strip, the results of which were compared with the results obtained from the model without the inclusion of membrane residual stresses. Fig. 8 shows the comparison of moment-curvature responses obtained from the beam models for specimen 125×85×6.5-4C with and without the inclusion of membrane residual stresses. This comparison supports that the influence of residual stresses on the structural response

of cold-formed steel SOHS beam is negligible. For simplification, bending and membrane residual stresses were not explicitly included in the FE model.

Due to the cold-work induced during fabrication, significant strength enhancement exists in the corner regions. However, the strength enhancement is not limited to the corner regions, but extended to a certain distance away from the corners. Therefore, the sensitivity analysis on corner region extension was conducted to determine the length of extension. The corner was extended by t, $2t$ and $2.5t$ in the sensitivity analysis. Table 4 summarizes the comparison results of the sensitivity analysis and shows that different corner extensions provide similar prediction with only 1% on average. The value of corner region extension was taken to be $2t$ in the numerical models, which was consistent with the value adopted for the cold-formed steel SOHS stub column FE model [7] and echoed with the commonly adopted value suggested by previous researchers [23-26].

The initial local geometric imperfection pattern was taken as the lowest elastic local buckling mode shape by eigenvalue analysis and the buckling mode was amplified by a certain magnitude of imperfection. The sensitivity study was also performed to determine the suitable magnitude of the local imperfections to be adopted in the model validation and further parametric study. Three magnitudes of local imperfection were considered in the sensitivity study, namely $t/16$, $t/50$ and $t/100$. From the results shown in Table 4, the models with different magnitudes of local imperfection provide similar predictions with only 1% difference on average. The magnitude of $t/50$ was selected for local imperfection, as consistently adopted for the cold-formed steel SOHS stub column model [7].

4. Validation of finite element models

Based on the aforementioned modeling parameters and assumptions, the finite element models of beam members were developed and validated against 20 beam tests. The validation results as shown in the second last column of Table 4 indicate that the finite element models can successfully replicate the flexural capacities of the beam specimens as evident by the mean value and coefficient

of variation (COV) of the test-to-FE strength ratio of 1.02 and 0.050, respectively. Comparisons between the experimental and numerical moment-curvature and moment-rotation responses for typical test specimens are depicted in Fig. 9. The failure modes can also be captured by the finite element predictions as shown in Figs. 10 and 11.

5. Parametric study

The validated finite element model for four-point bending test was used to perform extensive parametric study on cold-formed steel SOHS under constant moment. Finite element analyses on a total of 198 beam specimens were conducted, where 99 beam specimens were bent about the major axis in positive direction and the rest of the specimens were bent in negative direction. Extensive range of cross-section geometries was designed for the parametric study. The cross-section aspect ratio of the SOHS varied from 1.25 to 2.50. The overall depth of the section varied from 140 to 450 mm. The thickness of the section was designed to cover a spectrum of slenderness ratio from stocky to slender sections. The shear span was carefully designed to avoid the occurrence of shear failure, and the moment span was taken as the maximum of 3 times the overall depth of SOHS and the length of the designed shear span. The moment capacities obtained from the finite element analyses are summarized in Table 5. The results obtained from numerical study together with the experimental results were used in the assessment of existing and modified design rules.

6. Reliability analysis

The test and finite element strengths were only compared with the design strengths predicted by the Direct Strength Method as detailed in the North American Specification AISI S100-16 [11] and the Continuous Strength Method [14-16]. The reliability of these two design methods for flexural strength predictions of cold-formed steel SOHS beams was evaluated by reliability analysis as detailed in the North American Specification AISI S100-16 [11]. The targeted value of reliability index (β) of 2.5 was taken as the lower limit in this study. The design method is considered to be

reliable if the reliability index is larger than or equal to 2.5. The values of statistical parameters included in the calculation of reliability index are specified in the AISI S100-16 [11]. The calibration coefficient in the reliability index calculation depends on the load combination specified in different design specifications and the load combinations of 1.2DL+1.6LL and 1.35DL+1.5LL were used in the reliability analysis for the Direct Strength Method and the Continuous Strength Method, respectively, where DL and LL mean the dead load and live load, respectively. The values of resistance factor ϕ are 0.9 and 1.0 for the Direct Strength Method and the Continuous Strength Method, respectively. The values of other statistical parameters (M_m=1.1, F_m=1.0, V_M=0.1, V_F=0.05 and V_Q=0.21) are specified in the AISI S100-16 [11]. The reliability indices of each design rules for flexural strength predictions of cold-formed steel SOHS beam members are shown in Table 6.

7. Discussions and evaluations of the current design rules

7.1. General

The current design specifications for steel structures [10-13] do not cover the structural design for cold-formed steel SOHS. Therefore, the test strengths and FE flexural strengths obtained from parametric study were only compared with the nominal flexural strengths (unfactored design flexural strengths) of SOHS under constant moment predicted by the Direct Strength Method [11] and the Continuous Strength Method [14-16]. The material properties at the location with lowest 0.2% proof stress were used in nominal strength calculation for conservative predictions.

7.2. Direct strength method

The Direct Strength Method for beam design is detailed in Chapter F of the AISI S100-16 [11]. Unlike the traditional design approaches, the DSM does not require the classification of each component in the section and the iterative effective width calculation. Although the DSM design equations were originally calibrated by open sections with flat plate elements, the applicability of the DSM for the newly developed cold-formed steel semi-oval hollow section beams is assessed in this study. In the Direct Strength Method, the finite strip method employed in CUFSM program [27] was used to determine the critical elastic buckling moments of SOHS for local buckling and distortional

buckling scenarios with a 1 mm half-wave length interval. Followed by critical elastic buckling moments determination, the nominal flexural strengths for lateral-torsional buckling, local buckling and distortional buckling were calculated according to Sections F2.1, F3.2.1 and F4.1 of the AISI S100-16 [11], respectively. No lateral-torsional buckling was observed from the tests and finite element analyses. The nominal moment capacity of the semi-oval hollow section (M_{DSM}) is taken as the minimum of the nominal flexural strengths for local buckling and distortional buckling. The mean value of M_u/M_{DSM} is 1.43 with the corresponding COV of 0.164. The reliability index is 3.38, which is larger than 2.5. It is found that the Direct Strength Method provides very conservative and scattered predictions for SOHS beam members in a reliable manner. The comparison of test and numerical results with the design strengths predicted by the DSM is shown in Figs. 12 and 13.

For the design approach considering inelastic reserve capacity in the Direct Strength Method, the moment capacity ($M_{DSM,IR}$) was calculated according to Sections F2.4.2, F3.2.3 and F4.3 of the AISI S100-16 [11]. It is shown that the mean value of $M_u/M_{DSM,IR}$ is 1.20 with the corresponding COV of 0.080, which is less conservative and less scattered than the flexural strength predictions without considering inelastic reserve capacity (M_{DSM}). The reliability index of 3.21 was obtained, which is larger than 2.5. The comparison of flexural strengths obtained from test and finite element analyses with the design strengths predicted by the DSM with consideration of inelastic reserve capacity is shown in Fig. 14.

Although the Direct Strength Method with and without consideration of inelastic reserve capacity provide reliable flexural strength predictions, both approaches of the existing Direct Strength Method cannot accurately predict the design flexural strengths for cold-formed steel SOHS beams. It is therefore necessary to propose modification to the current Direct Strength Method in order to improve the accuracy of flexural strength predictions.

7.3. Continuous Strength Method

The Continuous Strength Method (CSM) is a deformation-based design approach [14-16] with

rational exploitation of the strain hardening of the metallic material and with the consideration of element interaction. Similar to the DSM, the design strength prediction by the CSM does not involve the cross-section classification and effective width calculation. There are two key components in the CSM, one is the material model considering the nonlinearity of different materials and another is the based curve defining the strain capacity for different section types. The material model for cold-formed structural steel section proposed by Buchanan *et al*. [15] was adopted herein for cold-formed steel SOHS. As a newly emerged cross-section type, there is no base curve available for semi-oval hollow sections investigated in this study. The applicability of the existing rectangular hollow section (RHS) and circular hollow section (CHS) approaches of the CSM using the corresponding base curves as shown in Eqs. (1) and (2) was assessed. The critical elastic buckling stress of SOHS for local buckling involved in the cross-section slenderness (λ_{CSM}) calculation was determined by the finite strip method employed in CUFSM program [27] with a 1 mm half-wave length interval. The upper limit of cross-section slenderness of 0.6 for CHS approach of the CSM was released in the assessment.

$$\left(\frac{\varepsilon_{csm}}{\varepsilon_y}\right)_{RHS} = \begin{cases} \frac{0.25}{\lambda_{CSM}^{3.6}} \leq \text{lesser}\left(15, \frac{0.4\varepsilon_u}{\varepsilon_y}\right) & \text{for } \lambda_{CSM} \leq 0.68 \\ \left(1 - \frac{0.195}{\lambda_{CSM}^{0.8}}\right)\frac{1}{\lambda_{CSM}^{0.8}} & \text{for } \lambda_{CSM} > 0.68 \end{cases} \quad (1)$$

$$\left(\frac{\varepsilon_{csm}}{\varepsilon_y}\right)_{CHS} = \begin{cases} \frac{4.44\times10^{-3}}{\lambda_{CSM}^{4.5}} \leq \text{lesser}\left(15, \frac{0.4\varepsilon_u}{\varepsilon_y}\right) & \text{for } \lambda_{CSM} \leq 0.3 \\ \left(1 - \frac{0.224}{\lambda_{CSM}^{0.342}}\right)\frac{1}{\lambda_{CSM}^{0.342}} & \text{for } 0.3 < \lambda_{CSM} \leq 0.6 \end{cases} \quad (2)$$

For the nominal flexural strengths predicted by the RHS and CHS approaches of the Continuous Strength Method, the mean values of $M_u/M_{CSM,RHS}$ and $M_u/M_{CSM,CHS}$ are 1.15 and 1.34 with the corresponding COV values of 0.103 and 0.156, respectively. With the resistance factor of 1.0, the resulted reliability indices are 2.37 and 2.70 for RHS and CHS approaches of the CSM, respectively. These indicate that the flexural strength predictions by the RHS approach are not reliable, whilst the predictions by the CHS approach are reliable. It is found that the two approaches in the CSM provide quite conservative and scattered predictions for SOHS beam members. The comparisons of test and finite element analysis results with the design strengths predicted by the RHS

and CHS approaches of the CSM are shown in Fig. 15. Modification on the Continuous Strength Method for cold-formed steel SOHS beam members to improve the accuracy of design strength predictions remains possible.

8. Modified design methods and comparison of flexural strengths

8.1. Modified Direct Strength Method

The applicability of the existing design equations, which were originally calibrated by open sections with flat plate elements, for cold-formed steel SOHS beam members was assessed in previous section. It was found that the DSM can be modified for cold-formed steel SOHS beam members to improve the accuracy of design strength predictions. From Fig. 12, it is clear that the predictions for sections bent in positive direction, which involves distortional bucking mode, and compact sections bent in negative direction are conservative since the existing DSM assumes linear elastic stress distribution in the section and ignores the possible elastic-plastic distribution for non-slender sections. Hence, modification to DSM is proposed in this study.

The slenderness factors for local (λ_l) and distortional buckling (λ_d) of beam are defined in Eqs. (3) and (4), respectively.

$$\lambda_l = \sqrt{\frac{M_y}{M_{crl}}} \tag{3}$$

$$\lambda_d = \sqrt{\frac{M_y}{M_{crd}}} \tag{4}$$

where M_y is the yield moment of beam, M_{crl} and M_{crd} are critical elastic buckling moments for local and distortional buckling, respectively.

The design strength predicted by the modified Direct Strength Method (M_{DSM}*) is taken as the minimum of M_{ne}*, M_{nl}* and M_{nd}* calculated as per Eqs. (5)-(7), which consider the inelastic moment capacity, effects of local buckling and distortional buckling, respectively.

$$M_{ne}{}^{*} = 1.6M_y \tag{5}$$

$$M_{nl}{}^{*} = \begin{cases} 1.6M_y & \text{for } \lambda_l \leq 0.47 \\ \left[1 - 0.04\left(\frac{M_{crl}}{M_y}\right)^{0.36}\right]\left(\frac{M_{crl}}{M_y}\right)^{0.36} M_y & \text{for } \lambda_l > 0.47 \end{cases} \quad (6)$$

$$M_{nd}{}^{*} = \begin{cases} 1 - 1.25(\lambda_d - 0.673) \leq 1.6M_y & \text{for } \lambda_d \leq 0.673 \\ \left[1 - 0.22\left(\frac{M_{crd}}{M_y}\right)^{0.5}\right]\left(\frac{M_{crd}}{M_y}\right)^{0.5} M_y & \text{for } \lambda_d > 0.673 \end{cases} \quad (7)$$

To assess the applicability of the modified Direct Strength Method for design strength predictions of cold-formed steel SOHS subjected to pure bending about the major axis, the mean value and COV of M_u/M_{DSM}* were evaluated and the reliability analysis was conducted. From the comparison results as shown in Table 6 and Fig. 16, it is found that the modified DSM provides better design strength prediction as evident by the mean values and COV of M_u/M_{DSM}* of 1.05 and 0.069, respectively. The resistance factor of 0.9 is proposed, and the reliability index of 2.7 was obtained, which is larger than the targeted value of 2.5 indicating that the modified DSM is reliable in predicting the flexural strengths of cold-formed steel SOHS subjected to major axis bending. The modified DSM not only provides reliable strength predictions for cold-formed steel SOHS under pure bending, but also provides the most accurate and the least scattered predictions among these design rules.

8.2. Modified Continuous Strength Method

The base curve, as one of the key components in the CSM, is only available for rectangular and circular hollow sections. The base curves for RHS and CHS were shown to be quite conservative in the nominal flexural strength predictions for cold-formed steel SOHS under constant moment in previous section of this paper.

Modified base curve has been proposed by Chen and Young [7] as expressed by Eq. (8) for semi-oval hollow sections. To evaluate the effectiveness of the CSM incorporating the modified base curve for SOHS beam members, the experimental and numerical results were compared with the design predictions by the modified CSM as shown in Table 6 and Fig. 17. The accuracy of nominal flexural strength predictions is improved by adopting the modified CSM. The mean M_u/M_{CSM}* is 1.07

and the corresponding COV is 0.096. The reliability index is 2.51 with the proposed resistance factor of 0.9, indicating that the modified CSM is reliable.

$$\left(\frac{\varepsilon_{csm}}{\varepsilon_y}\right)_{SOHS} = \begin{cases} \frac{0.555}{\lambda_{CSM}^{3.9}} \leq \text{lesser}\left(15, \frac{0.4\varepsilon_u}{\varepsilon_y}\right) & \text{for } \lambda_{CSM} \leq 0.86 \\ \left(1 - \frac{0.09}{\lambda_{CSM}^{0.7}}\right)\frac{1}{\lambda_{CSM}^{0.7}} & \text{for } \lambda_{CSM} > 0.86 \end{cases} \quad (8)$$

9. Conclusions

Comprehensive experimental and numerical investigation has been performed to study the beam behavior of cold-formed steel semi-oval hollow sections. A total of 20 beam tests was conducted on semi-oval hollow sections subjected to bending about the major axis in positive and negative directions under constant moment and a moment gradient. Finite element models were developed and validated against the test results. Parametric study, which covered a wide range of cross-section geometries, was carried out to investigate the behavior of cold-formed steel semi-oval hollow sections under constant moment numerically. The results obtained from the experimental program and numerical study were used to evaluate the existing and modified Direct Strength Methods and Continuous Strength Methods. The test and finite element strengths were compared with the predicted strengths by existing and modified design methods and reliability analysis was conducted. The comparison results show that the existing Direct Strength Method with and without consideration of inelastic reserve capacity as well as the rectangular hollow section approach and circular hollow section approach as based curves in the Continuous Strength Method provide quite conservative and scattered predictions. Therefore, modifications on the Direct Strength Method and the Continuous Strength Method are proposed. With the modified design equations and proposed resistance factor, the modified Direct Strength Method and Continuous Strength Method are capable to provide reliable design strength predictions with improved accuracy. It is recommended to use either the modified Direct Strength Method or modified Continuous Strength Method for the flexural strength predictions of cold-formed steel semi-oval hollow sections under pure bending.

References

[1] Lai MH, Ho JCM. A theoretical axial stress-strain model for circular concrete-filled-steel-tube columns. Engineering Structures 2016;125:124-143.

[2] Lai MH, Ho JCM. An analysis-based model for axially loaded circular CFST columns. Thin-Walled Structures 2017;119:770-781.

[3] Chen MT, Young B. Tests of cold-formed steel elliptical hollow section beams. In: 7th International Conference on Coupled Instabilities in Metal Structures, Baltimore, Maryland, U.S.; Paper No. 48.

[4] Chen MT, Young B. Structural performance of cold-formed steel elliptical hollow section pin-ended columns. Thin-Walled Structures 2019;136:267-279.

[5] Quach WM, Young B. Material properties of cold-formed and hot-finished elliptical hollow sections. Advances in Structural Engineering 2015;18(7):1101-1114.

[6] Chan TM, Huai YM, Wang W. Experimental investigation on lightweight concrete-filled cold-formed elliptical hollow section stub columns. Journal of Constructional Steel Research 2015;115:434-444.

[7] Chen MT, Young B. Cross-sectional behavior of cold-formed steel semi-oval hollow sections. Engineering Structures 2018;177:318-330.

[8] Chen MT, Young B. Experimental and numerical investigation on pin-ended cold-formed steel semi-oval hollow section compression members. Journal of Constructional Steel Research 2018;151:174-184.

[9] Chen MT, Young B. Experimental study on cold-formed steel semi-oval hollow section columns. In: 16th International Symposium on Tubular Structures, Melbourne, Australia; p. 549-556.

[10] ANSI/AISC360 2016. Specification for Structural Steel Buildings. *ANSI/AISC 360-16.* Chicago, IL, USA: American Institute of Steel Construction.

[11] AISI-S100 2016. North American Specification for the design of cold-formed steel structural members. *AISI S100-16.* Washington,D.C., USA: American Iron and Steel Institute.

[12] AS/NZS4600 2005. Cold-formed steel structure. *AS/NZS 4600:2005.* Sydney, Australia: Standards Australia/Standards New Zealand.

[13] EN 1993-1-1:2005. Design of steel structures–Part 1.1: General rules and rules for buildings. Brussels, Belgium: European Committee for Standardization; 2005.

[14] AISC 2013. Structural Stainless Steel. *AISC Design Guide 30.* American Institute of Steel Construction.

[15] Buchanan C, Gardner L, Liew A. The continuous strength method for the design of circular hollow sections. Journal of Constructional Steel Research 2016;118:207-216.

[16] Gardner L. The continuous strength method. Structures and Buildings 2008;161(3):127-133.

[17] Huang Y, Young B. Material properties of cold-formed lean duplex stainless steel sections. Thin-walled structures 2012;54:72-81.

[18] Ma JL, Chan TM, Young B. Material properties and residual stresses of cold-formed high strength steel hollow sections. Journal of Constructional Steel Research 2015;109:152-165.

[19] Young B, Lui W-M. Behavior of cold-formed high strength stainless steel sections. Journal of Structural Engineering 2005;131(11):1738-1745.

[20] Chen MT, Young B. Material properties and structural behavior of cold-formed steel elliptical hollow section stub columns. Thin-Walled Structures 2019;134:111-126.

[21] Huang Y, Young B. Experimental and numerical investigation of cold-formed lean duplex stainless steel flexural members. Thin-Walled Structures 2013;73:216-228.

[22] Huang Y, Young B. Structural performance of cold-formed lean duplex stainless steel columns. Thin-Walled Structures 2014;83:59-69.

[23] Ma JL, Chan TM, Young B. Experimental Investigation on Stub-Column Behavior of Cold-Formed High-Strength Steel Tubular Sections. Journal of Structural Engineering 2015;142(5):04015174.

[24] Zhao O, Rossi B, Gardner L, Young B. Behaviour of structural stainless steel cross-sections under combined loading–Part II: Numerical modelling and design approach. Engineering Structures 2015;89:247-259.

[25] Gardner L, Nethercot DA. Numerical modeling of stainless steel structural components - a consistent approach. Journal of Structural Engineering 2004;130(10):1586-1601.

[26] Ma JL, Chan TM, Young B. Design of cold-formed high strength steel tubular beams. Engineering Structures 2017;151:432-443.

[27] Schafer BW, Ádány S. Buckling analysis of cold-formed steel members using CUFSM: conventional and constrained finite strip methods. In: Eighteenth International Specialty Conference on Cold-Formed Steel Structures, Orlando, FL, USA; 2006. 39-54.

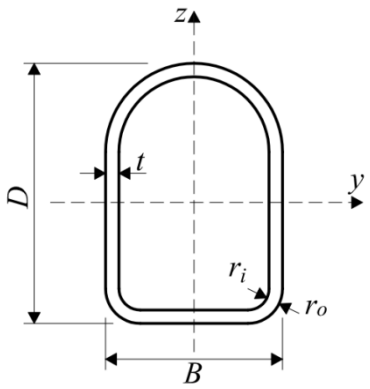

Fig. 1. Cross-section geometry of SOHS

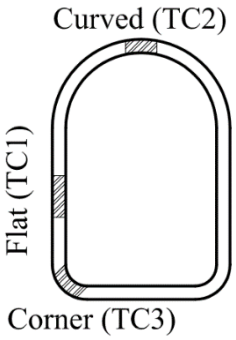

Fig. 2. Critical locations of tensile coupon specimens

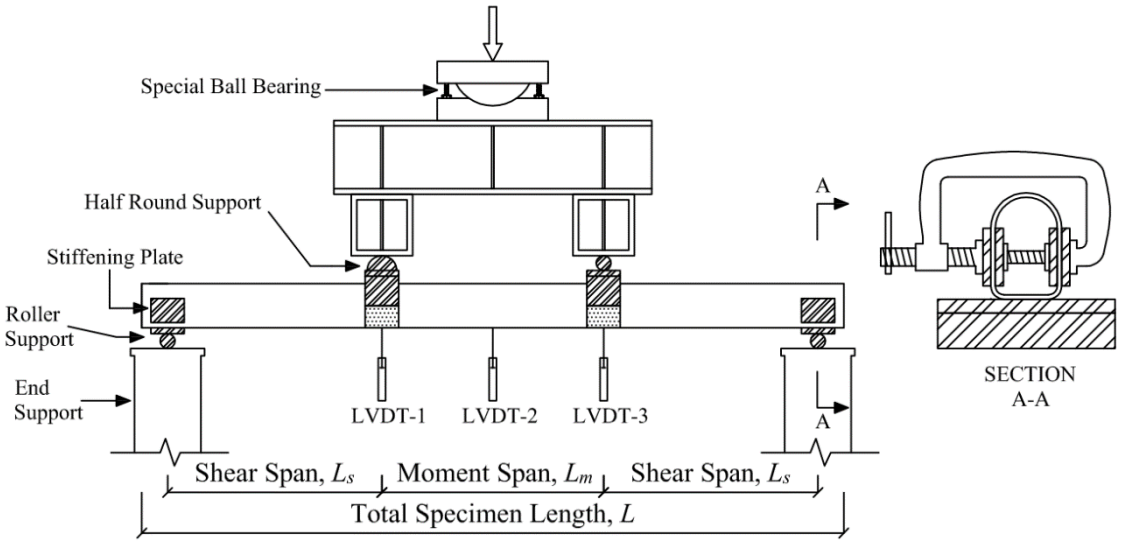

(a) Schematic setup of four-point bending test

(b) Experimental setup of four-point bending test

Fig. 3. Four-point bending test arrangement

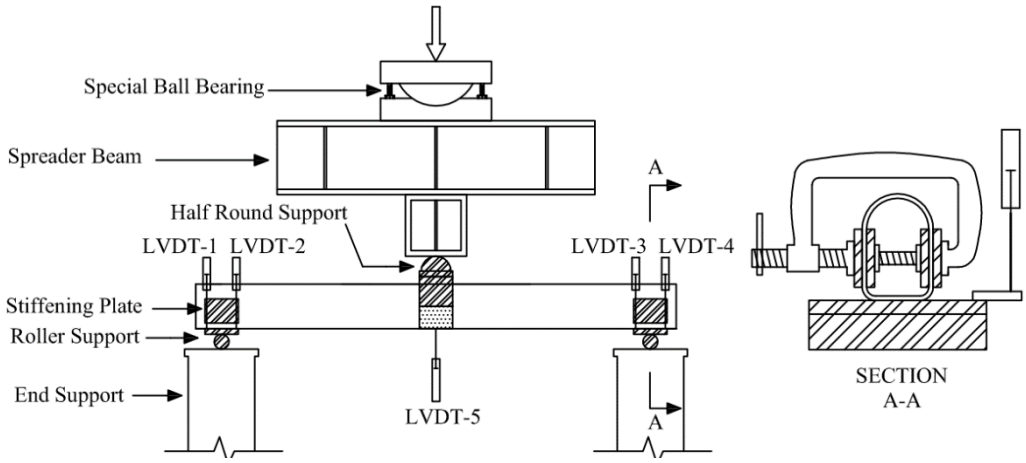

(a) Schematic setup of three-point bending test

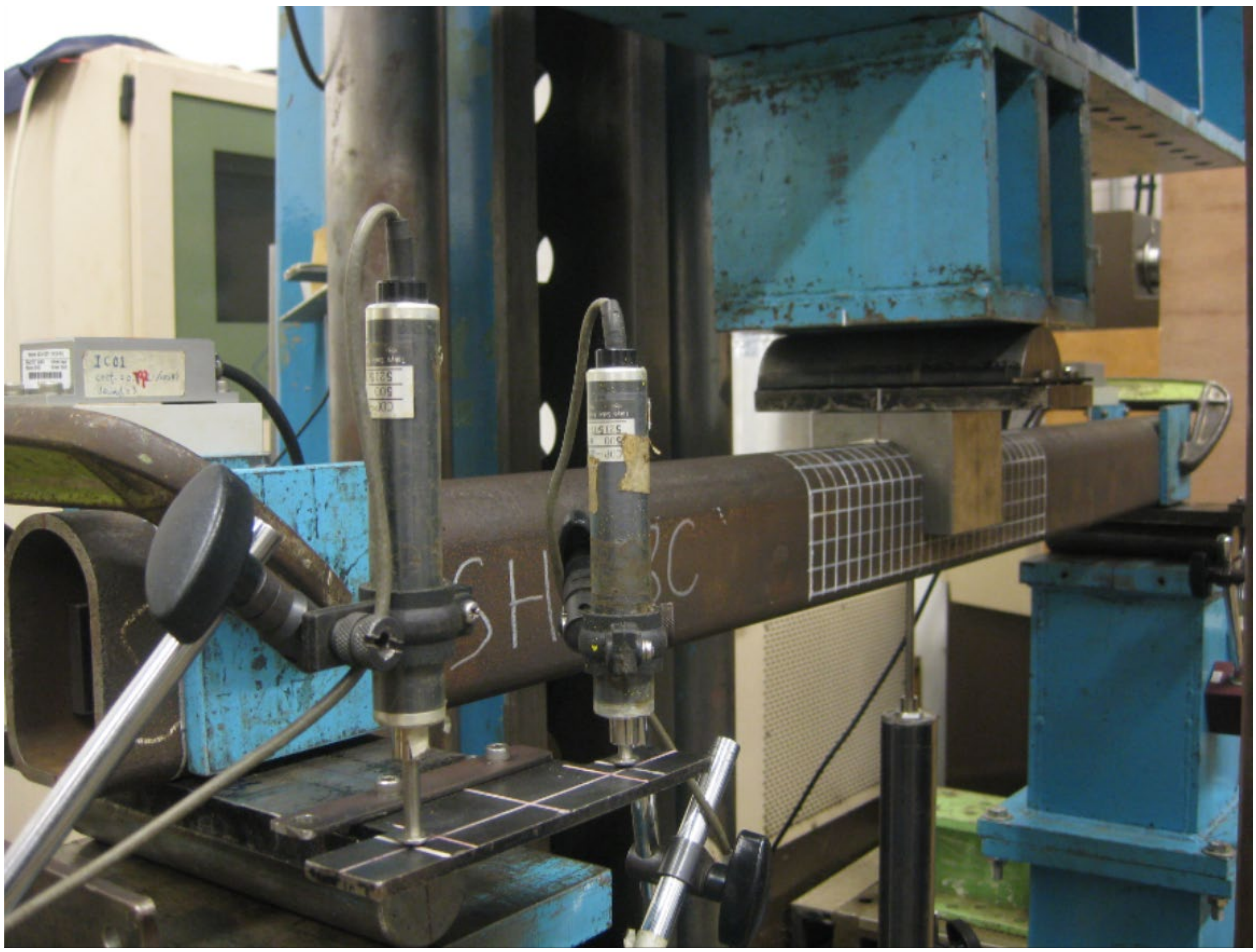

(b) Experimental setup of three-point bending test

Fig. 4. Three-point bending test arrangement

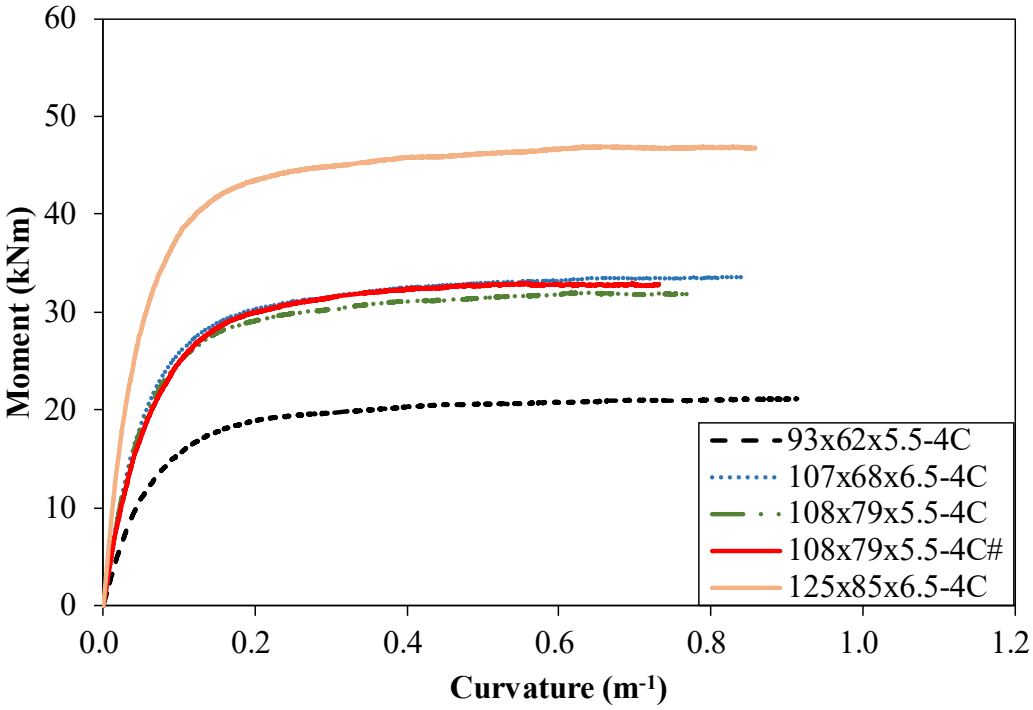

(a) Major axis bending in positive direction

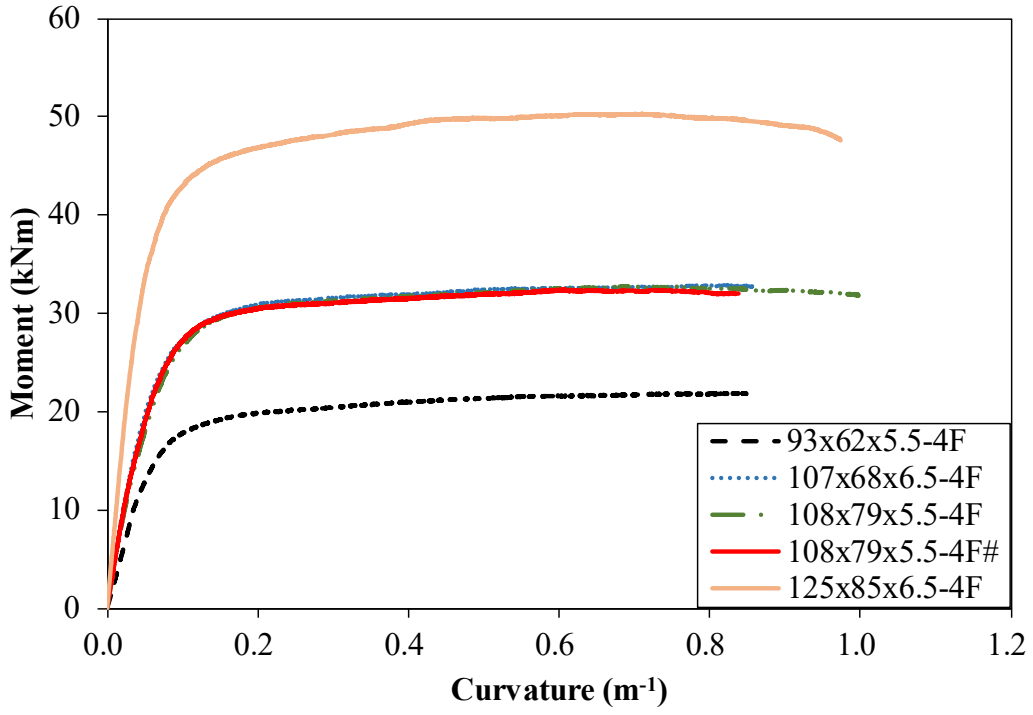

(b) Major axis bending in negative direction

Fig. 5. Moment-curvature relationships of SOHS flexural members subjected to four-point bending

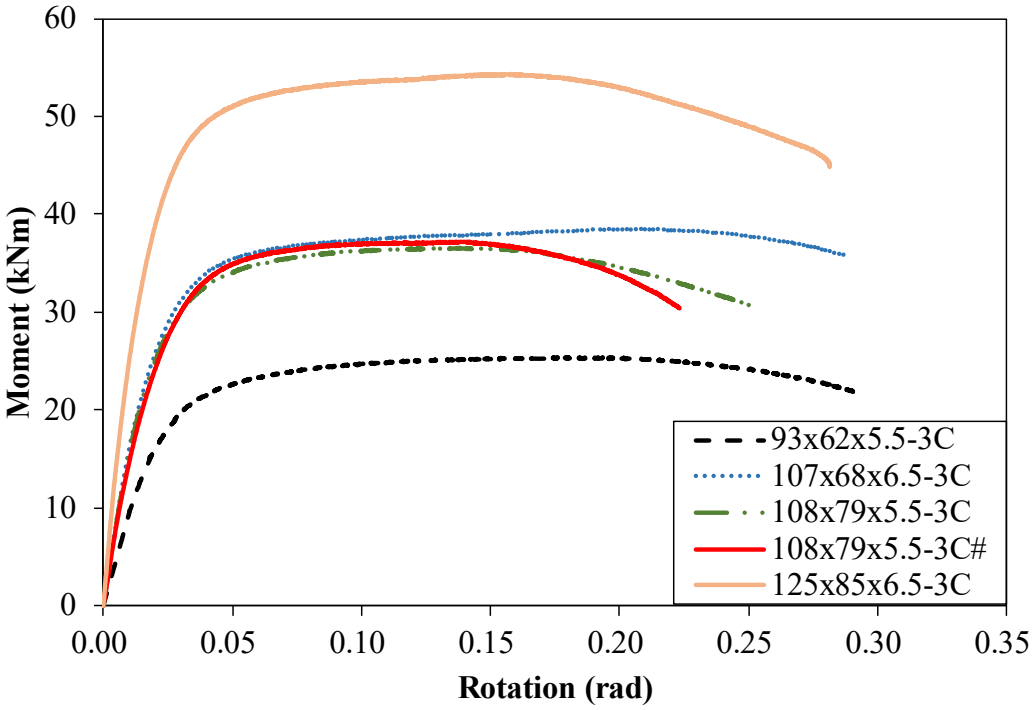

(a) Major axis bending in positive direction

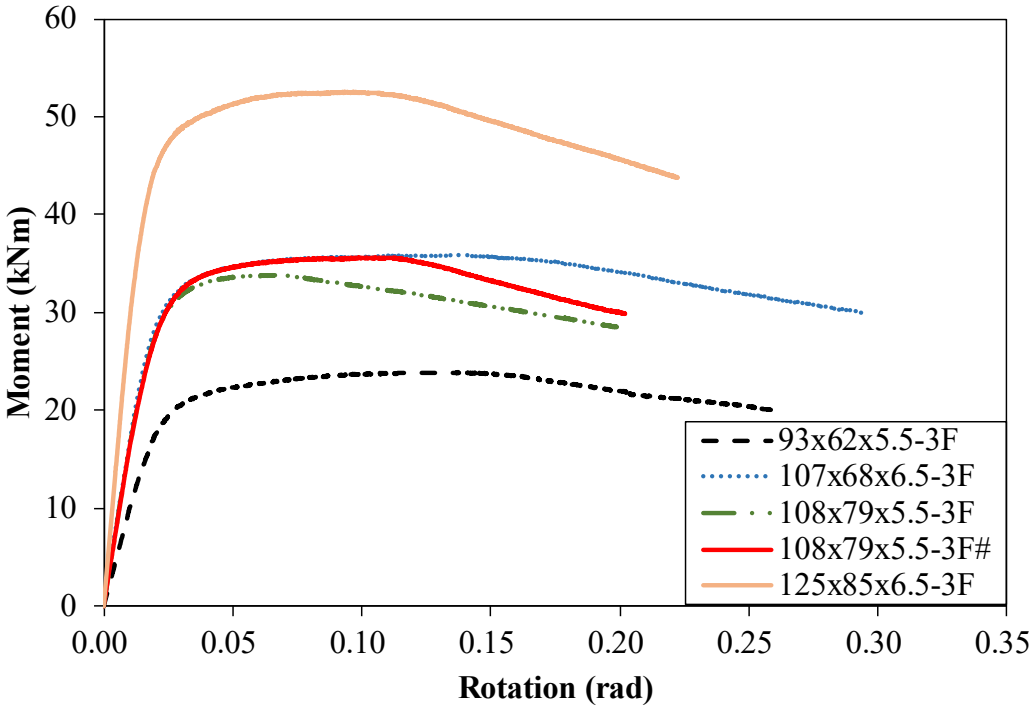

(b) Major axis bending in negative direction

Fig. 6. Moment-rotation relationships of SOHS flexural members subjected to three-point bending

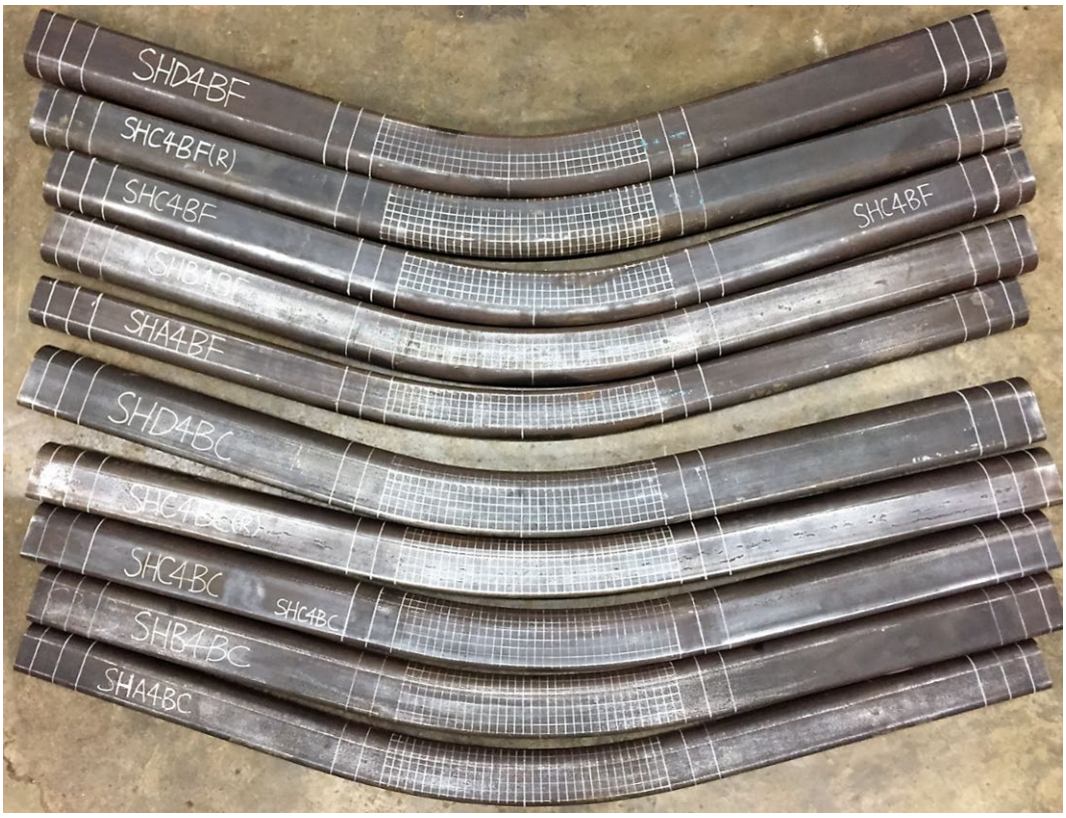

(a) Four-point bending

(b) Three-point bending

Fig. 7. Failed SOHS beam members

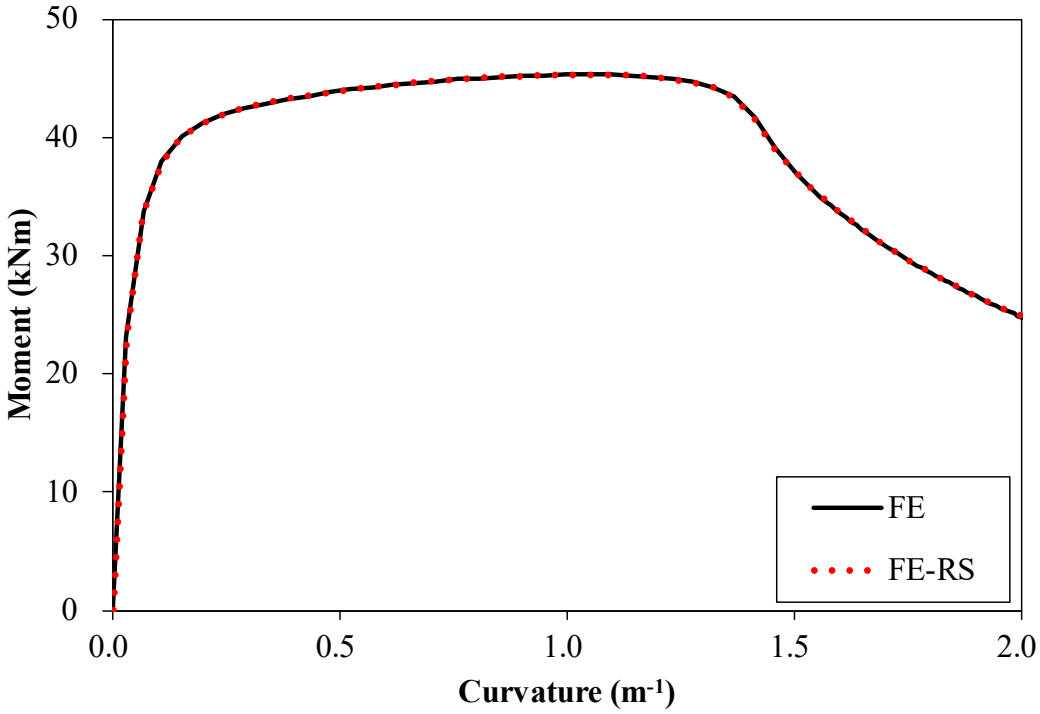

Fig. 8. Comparison of FE models of SOHS beam 125×85×6.5-4C with and without explicit inclusion of residual stresses

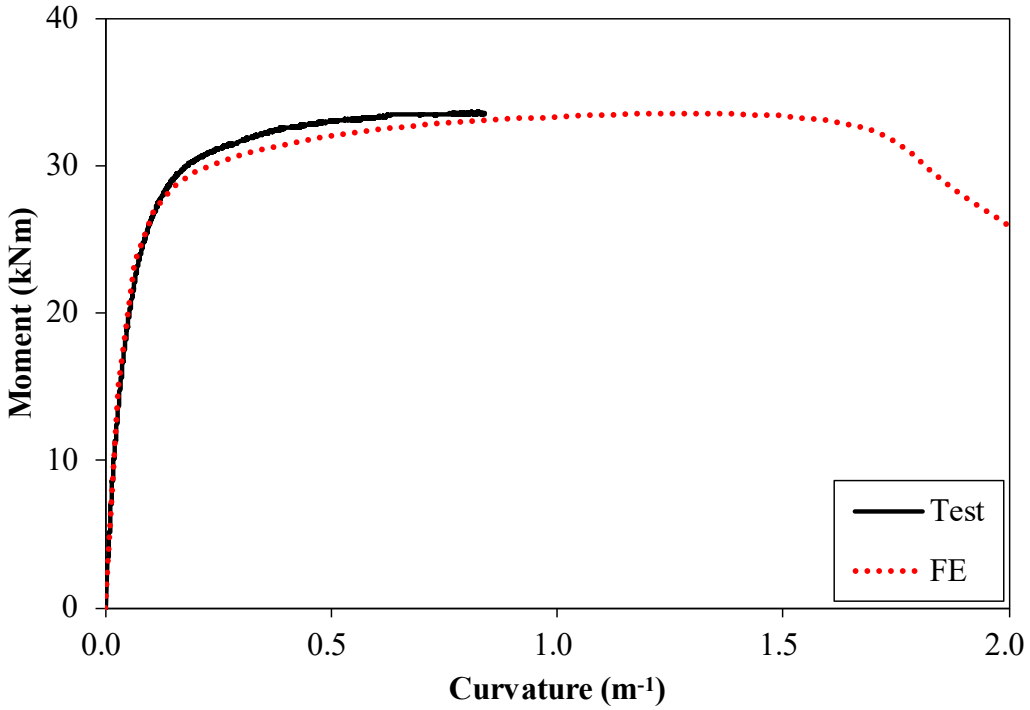

(a) Moment-curvature curves for beam specimen 107×68×6.5-4C

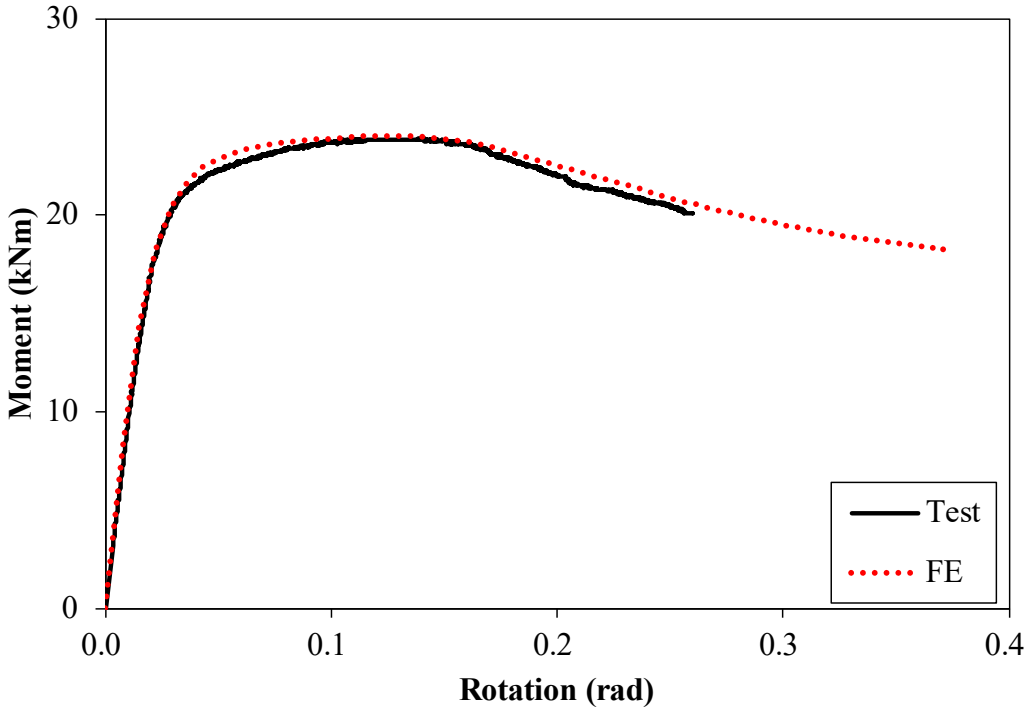

(b) Moment-rotation curves for beam specimen 93×62×5.5-3F

Fig. 9. Comparisons between experimental and numerical moment-curvature and moment-rotation responses for typical specimens

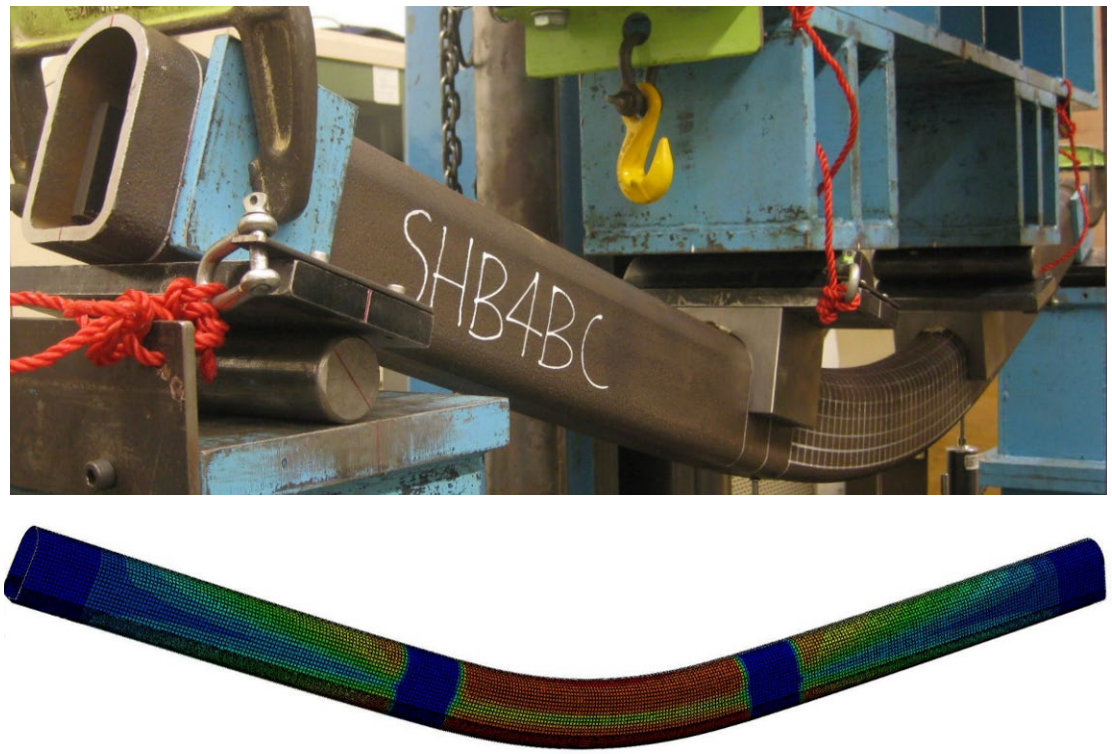

Fig. 10. Comparison between experimental and numerical failure modes for beam specimen 107×68×6.5-4C

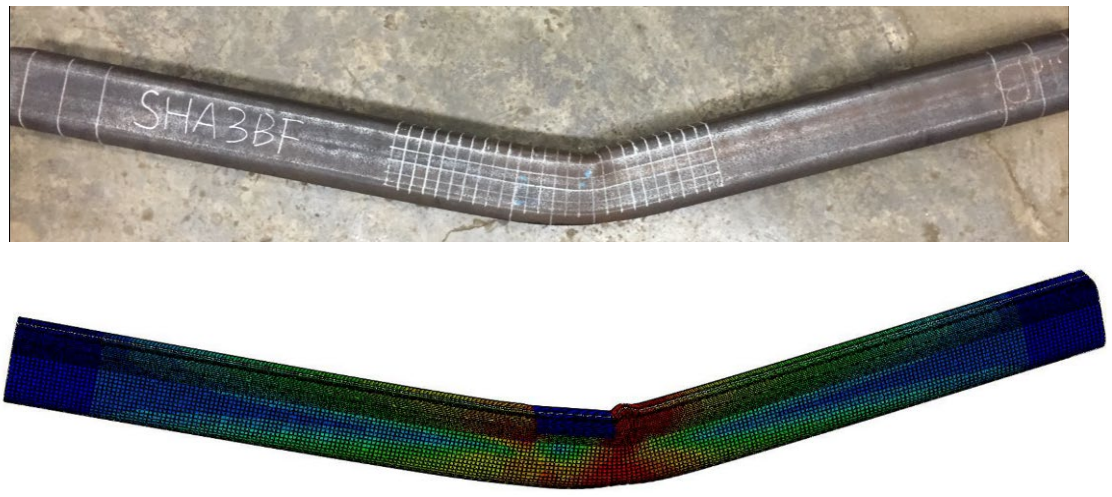

Fig. 11. Comparison between experimental and numerical failure modes for beam specimen 93×62×5.5-3F

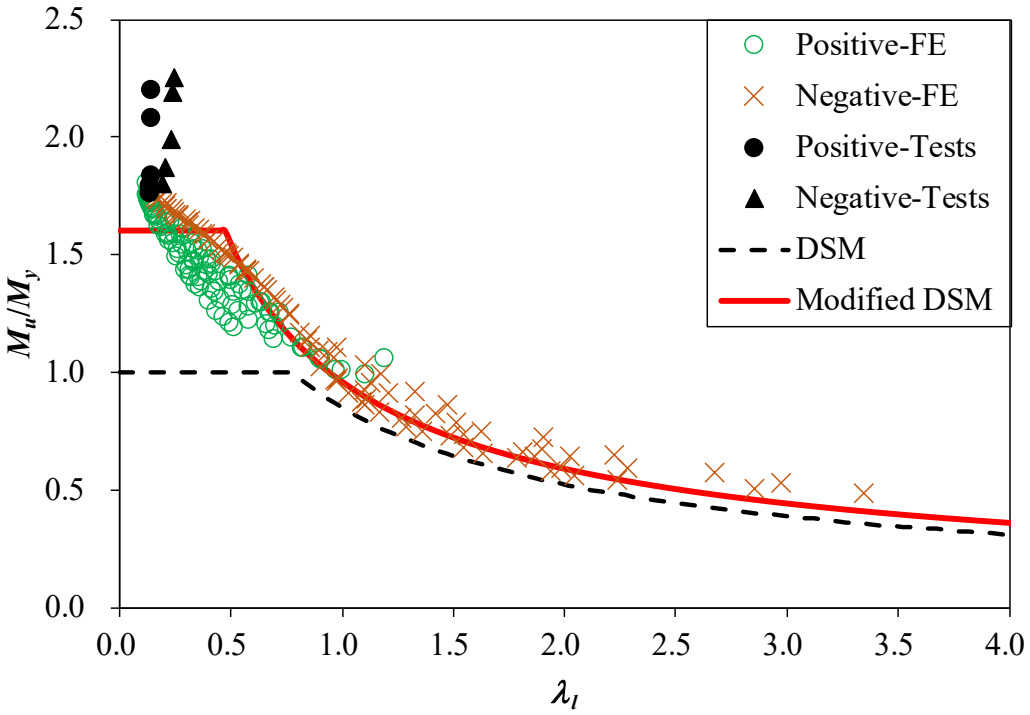

(a) Local buckling

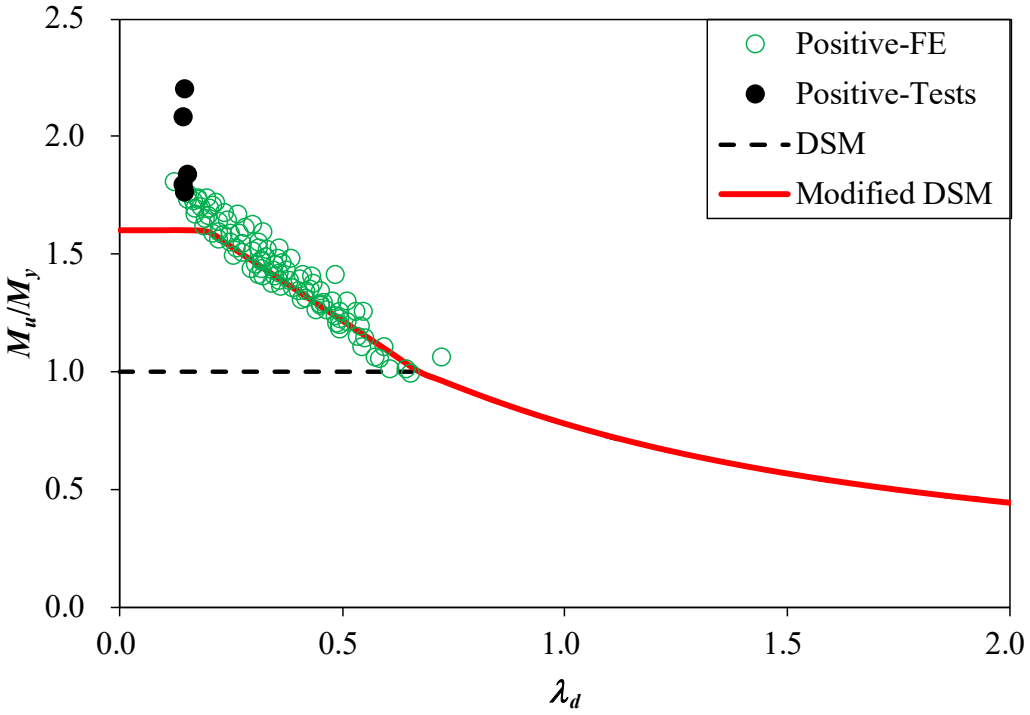

(b) Distortional buckling

Fig. 12. Comparison of experimental and numerical strengths with design strengths predicted by the DSM and modified DSM

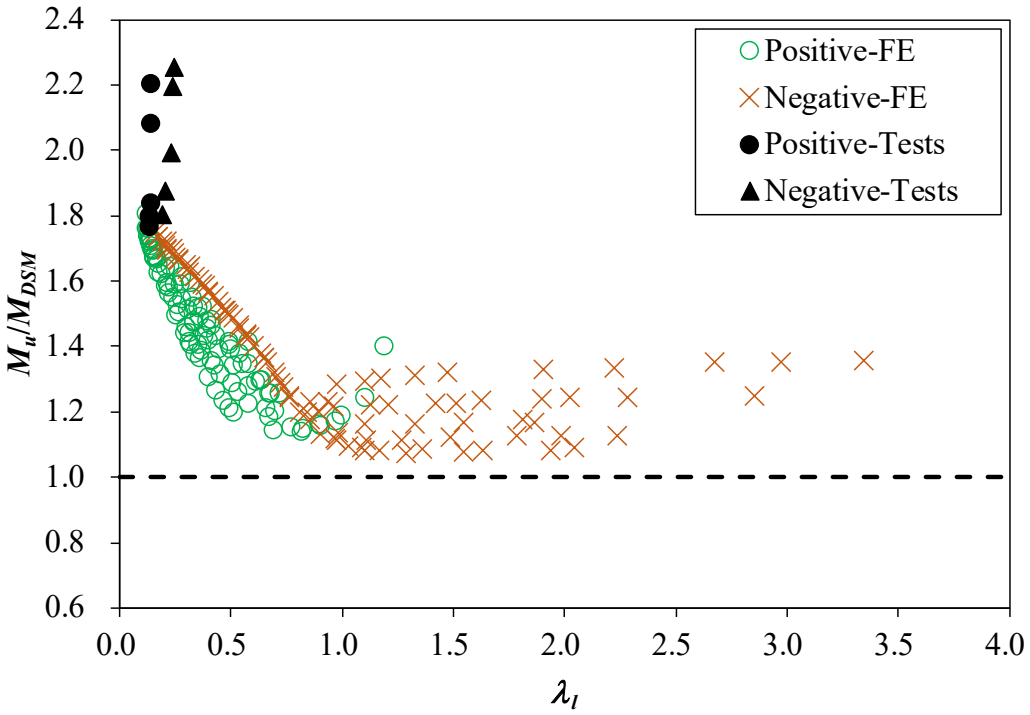

Fig. 13. Comparison of test and FE results with the DSM predictions without consideration of inelastic reserve capacity

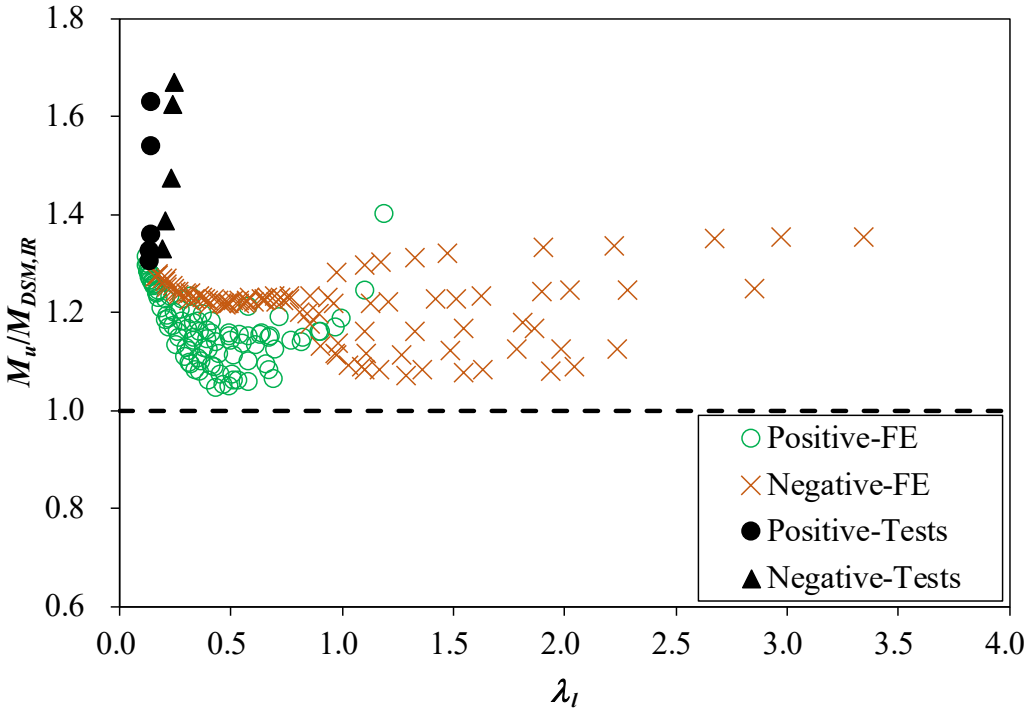

Fig. 14. Comparison of test and FE results with the DSM predictions with consideration of inelastic reserve capacity

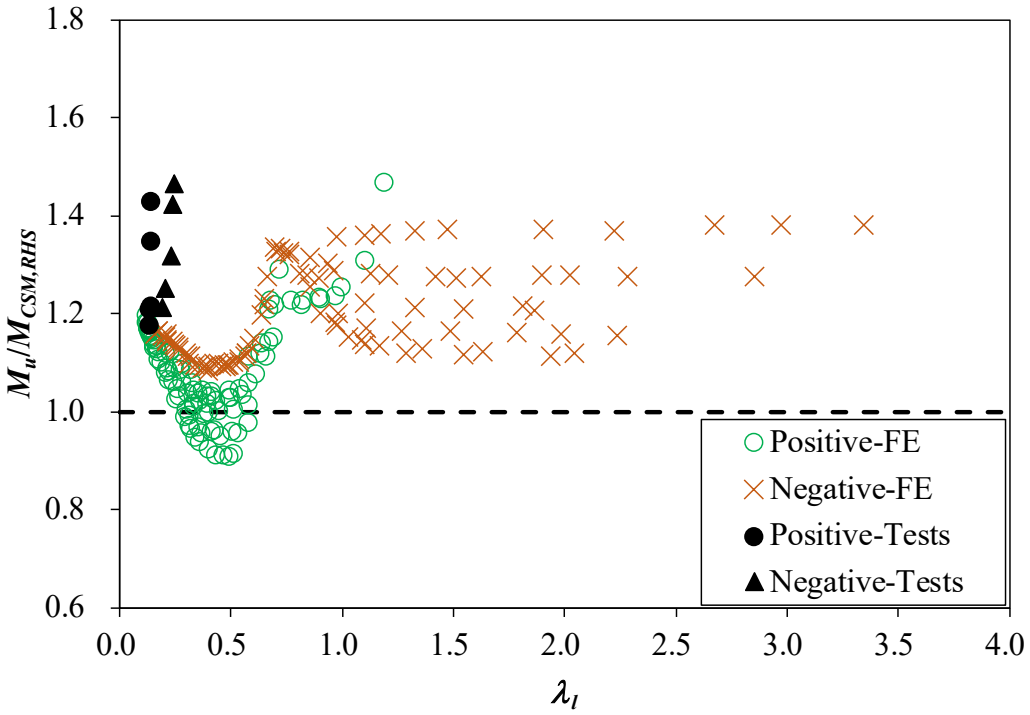

(a) RHS approach

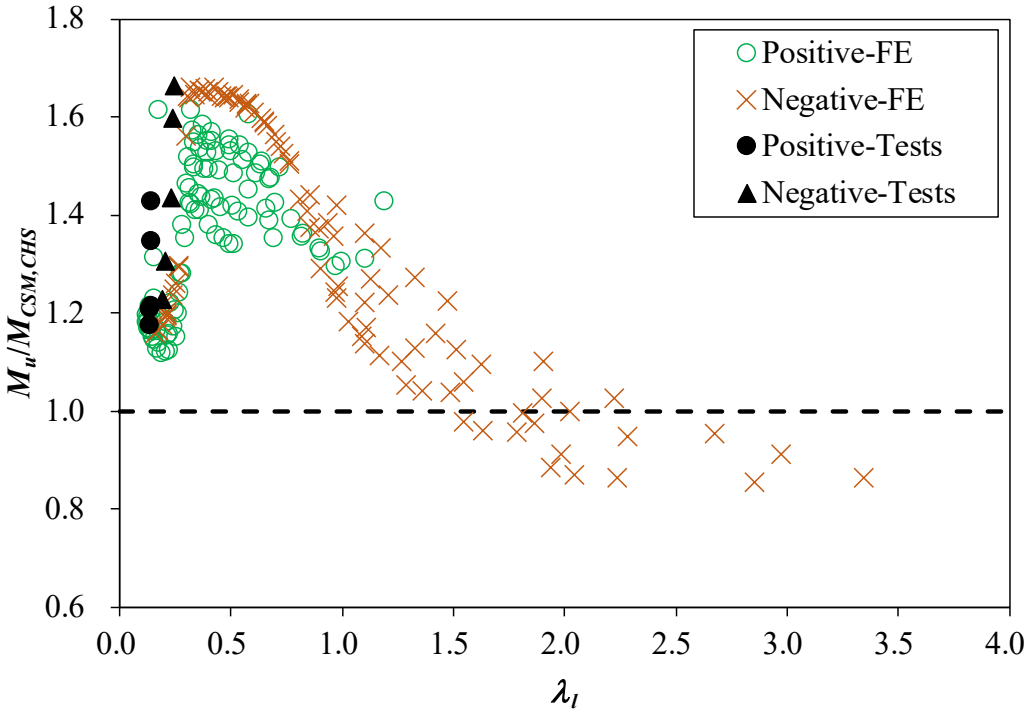

(b) CHS approach

Fig. 15. Comparison of test and FE results with the RHS and CHS approaches in the CSM predictions

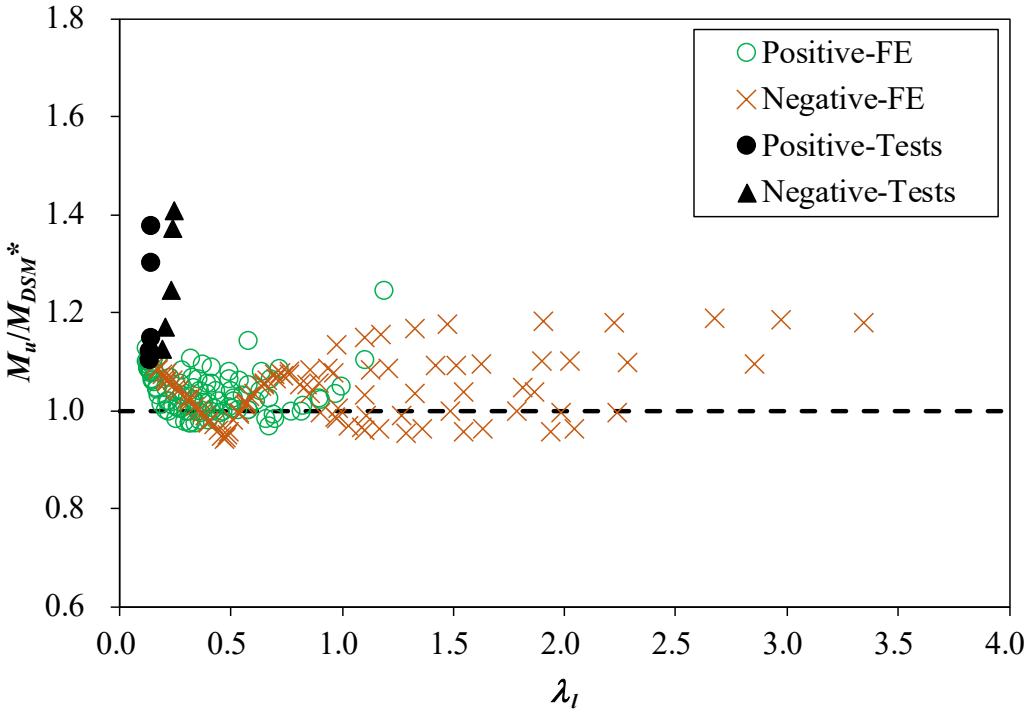

Fig. 16. Comparison of test and FE results with the modified DSM predictions

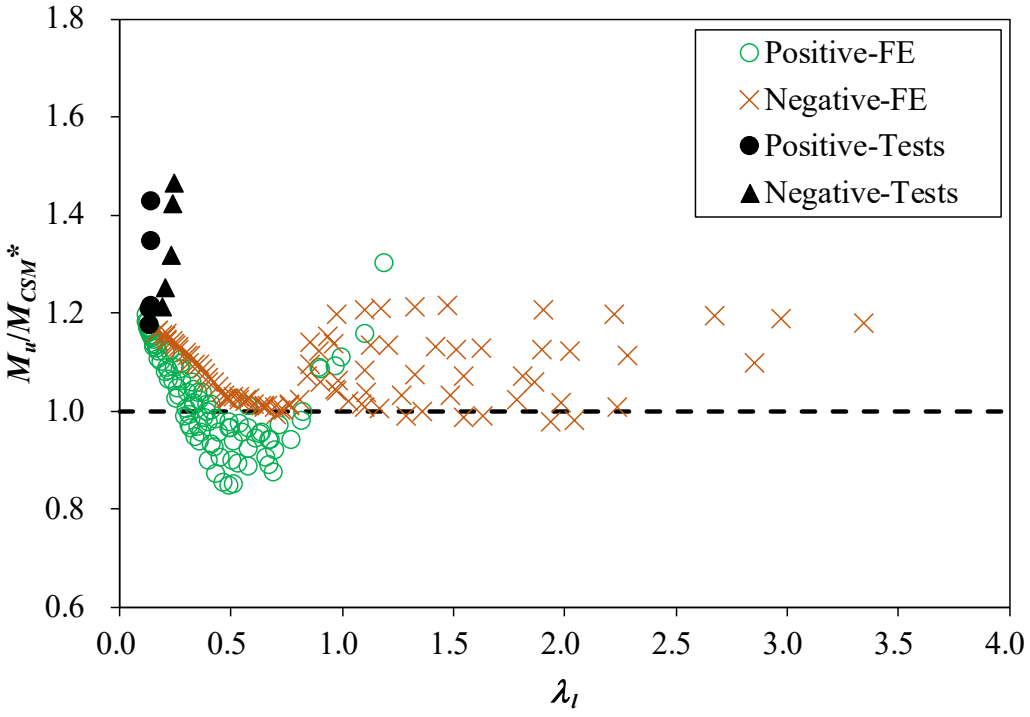

Fig. 17. Comparison of test and FE results with the modified CSM predictions

Specimen	Bending direction	D (mm)	B (mm)	t (mm)	r_o (mm)	r_i (mm)	L (mm)
93×62×5.5-4C	Positive	93.5	62.0	5.24	15.5	9.5	1900
107×68×6.5-4C	Positive	107.5	68.1	6.26	16.8	9.1	1900
108×79×5.5-4C	Positive	108.3	79.0	5.61	13.6	8.1	1900
108×79×5.5-4C#	Positive	108.4	78.9	5.44	13.0	6.6	1900
125×85×6.5-4C	Positive	124.8	85.0	6.36	17.6	9.5	1900
93×62×5.5-4F	Negative	93.4	62.1	5.04	14.5	9.5	1900
107×68×6.5-4F	Negative	107.3	68.1	6.09	16.3	8.8	1900
108×79×5.5-4F	Negative	108.5	79.1	5.21	13.8	7.5	1900
108×79×5.5-4F#	Negative	108.4	79.2	5.35	13.8	8.1	1900
125×85×6.5-4F	Negative	124.9	85.1	6.26	16.8	9.3	1900
93×62×5.5-3C	Positive	93.3	62.2	5.07	15.1	9.3	1300
107×68×6.5-3C	Positive	107.5	68.0	6.36	16.8	8.9	1300
108×79×5.5-3C	Positive	108.3	78.9	5.59	12.6	6.5	1300
108×79×5.5-3C#	Positive	108.5	79.2	5.35	13.4	6.9	1300
125×85×6.5-3C	Positive	124.9	85.1	6.63	17.9	9.9	1300
93×62×5.5-3F	Negative	93.3	62.1	5.35	14.6	9.0	1300
107×68×6.5-3F	Negative	107.3	67.9	6.44	17.5	8.8	1300
108×79×5.5-3F	Negative	108.3	79.1	5.47	13.3	7.3	1300
108×79×5.5-3F#	Negative	108.3	79.1	5.39	13.8	7.8	1300
125×85×6.5-3F	Negative	124.8	85.1	6.61	17.5	9.9	1300

Table 1. Measured dimensions of the beam specimens

Section	Flat (TC1)				Curved (TC2)				Corner (TC3)			
	E (GPa)	$\sigma_{0.2}$ (MPa)	σ_u (MPa)	ε_f (%)	E (GPa)	$\sigma_{0.2}$ (MPa)	σ_u (MPa)	ε_f (%)	E (GPa)	$\sigma_{0.2}$ (MPa)	σ_u (MPa)	ε_f (%)
93×62×5.5	204	453	549	22	211	444	551	23	211	511	600	16
107×68×6.5	211	475	548	20	209	450	540	26	210	518	605	16
108×79×5.5	206	460	555	27	199	366	545	26	185	507	625	17
125×85×6.5	207	439	530	26	204	419	531	28	203	486	577	19

Table 2. Measured material properties obtained from tensile coupon tests [7]

Specimens	$M_{Exp,3}$ (kNm)	Specimens	$M_{Exp,4}$ (kNm)	$\frac{M_{Exp,3}}{M_{Exp,4}}$
93×62×5.5-3C	25.4	93×62×5.5-4C	21.2	1.20
107×68×6.5-3C	38.6	107×68×6.5-4C	33.6	1.15
108×79×5.5-3C	36.6	108×79×5.5-4C	32.0	1.14
108×79×5.5-3C#	37.2	108×79×5.5-4C#	32.9	1.13
125×85×6.5-3C	54.4	125×85×6.5-4C	46.9	1.16
93×62×5.5-3F	23.9	93×62×5.5-4F	21.9	1.09
107×68×6.5-3F	35.9	107×68×6.5-4F	32.9	1.09
108×79×5.5-3F	33.8	108×79×5.5-4F	32.7	1.03
108×79×5.5-3F#	35.6	108×79×5.5-4F#	32.4	1.10
125×85×6.5-3F	52.6	125×85×6.5-4F	50.3	1.04
			Mean	1.11
			COV	0.046

Table 3. Test results and comparison

Specimen	M_{Exp}/M_{FE} Corner Extension (With no imperfection)			M_{Exp}/M_{FE} Local Imperfection (With 2t corner extension)		
	t	2t	2.5t	t/16	t/50	t/100
93×62×5.5-4C	0.98	0.98	0.97	0.98	**0.98**	0.98
107×68×6.5-4C	1.01	1.01	1.00	1.01	**1.01**	1.01
108×79×5.5-4C	0.98	0.98	0.97	0.98	**0.97**	0.97
108×79×5.5-4C#	1.05	1.04	1.03	1.04	**1.04**	1.04
125×85×6.5-4C	1.04	1.03	1.03	1.03	**1.03**	1.03
93×62×5.5-4F	1.07	1.07	1.07	1.08	**1.07**	1.07
107×68×6.5-4F	1.04	1.04	1.03	1.05	**1.04**	1.04
108×79×5.5-4F	1.10	1.10	1.09	1.11	**1.10**	1.10
108×79×5.5-4F#	1.07	1.06	1.06	1.08	**1.06**	1.06
125×85×6.5-4F	1.16	1.15	1.15	1.17	**1.15**	1.15
93×62×5.5-3C	1.08	1.07	1.07	1.07	**1.07**	1.07
107×68×6.5-3C	1.02	1.01	1.00	1.01	**1.01**	1.01
108×79×5.5-3C	0.98	0.97	0.96	0.97	**0.97**	0.97
108×79×5.5-3C#	1.03	1.02	1.02	1.02	**1.02**	1.02
125×85×6.5-3C	1.00	0.99	0.98	0.99	**0.99**	0.99
93×62×5.5-3F	1.00	0.99	0.99	1.00	**1.00**	0.99
107×68×6.5-3F	0.97	0.96	0.96	0.96	**0.96**	0.96
108×79×5.5-3F	0.96	0.95	0.95	0.96	**0.95**	0.95
108×79×5.5-3F#	1.02	1.02	1.02	1.03	**1.02**	1.02
125×85×6.5-3F	1.01	1.00	1.00	1.01	**1.01**	1.01
Mean	1.03	1.02	1.02	1.03	**1.02**	1.02
COV	0.049	0.048	0.049	0.053	**0.050**	0.049

Table 4. Summary of sensitivity study

Specimen	M_{FE} (kNm)	Specimen	M_{FE} (kNm)
450×360×20-F	2039.8	450×360×20-C	2094.9
450×360×16-F	1617.6	450×360×16-C	1681.0
450×360×5-F	324.6	450×360×5-C	485.3
450×360×3.5-F	180.7	450×360×3.5-C	325.5
450×360×2.5-F	102.9	450×360×2.5-C	222.0
450×360×2-F	70.1	450×360×2-C	172.5
450×300×16-F	1517.5	450×300×16-C	1554.9
450×300×12-F	1108.8	450×300×12-C	1164.5
450×300×8-F	664.1	450×300×8-C	756.7
450×300×4-F	213.6	450×300×4-C	351.7
450×300×3.5-F	171.4	450×300×3.5-C	299.9
450×300×2.5-F	97.4	450×300×2.5-C	201.6
450×300×2-F	66.5	450×300×2-C	151.1
450×225×20-F	1675.5	450×225×20-C	1700.1
450×225×16-F	1361.1	450×225×16-C	1382.4
450×225×6-F	427.2	450×225×6-C	488.1
450×225×4-F	201.3	450×225×4-C	306.6
450×225×3.5-F	161.1	450×225×3.5-C	258.3
450×225×2.5-F	92.3	450×225×2.5-C	159.0
450×225×2-F	63.1	450×225×2-C	117.4

450×200×16-F	1299.9	450×200×16-C	1319.3
450×200×10-F	800.7	450×200×10-C	823.9
450×200×4.5-F	248.6	450×200×4.5-C	333.8
450×200×3.5-F	158.0	450×200×3.5-C	238.8
450×200×3-F	122.4	450×200×3-C	188.4
450×200×2.5-F	90.0	450×200×2.5-C	144.5
450×200×2-F	61.8	450×200×2-C	109.4
450×180×16-F	1250.2	450×180×16-C	1266.8
450×180×10-F	774.8	450×180×10-C	795.6
450×180×5.5-F	366.3	450×180×5.5-C	394.8
450×180×4-F	201.1	450×180×4-C	269.0
450×180×3.5-F	156.7	450×180×3.5-C	228.7
450×180×2.5-F	89.0	450×180×2.5-C	132.9
450×180×2-F	61.2	450×180×2-C	112.1
420×240×20-F	1532.6	420×240×20-C	1558.5
420×240×8-F	578.9	420×240×8-C	626.4
420×240×6-F	384.4	420×240×6-C	455.0
420×240×3.5-F	150.7	420×240×3.5-C	247.9
420×240×2.5-F	85.9	420×240×2.5-C	157.3
350×200×12-F	650.0	350×200×12-C	662.0
350×200×8-F	418.0	350×200×8-C	440.4
350×200×4-F	153.8	350×200×4-C	205.6
350×200×3.5-F	118.0	350×200×3.5-C	177.1
350×200×2.5-F	67.6	350×200×2.5-C	117.7
300×240×8-F	346.1	300×240×8-C	371.1
300×240×6-F	234.8	300×240×6-C	273.0
300×240×4-F	128.4	300×240×4-C	176.0
300×240×2-F	41.2	300×240×2-C	80.4
300×240×1.5-F	25.5	300×240×1.5-C	58.2
300×200×16-F	662.4	300×200×16-C	675.9
300×200×6.5-F	256.8	300×200×6.5-C	277.6
300×200×4-F	123.9	300×200×4-C	163.7
300×200×2-F	39.4	300×200×2-C	74.9
300×150×6.5-F	239.5	300×150×6.5-C	247.9
300×150×4.5-F	151.4	300×150×4.5-C	165.3
300×150×3.5-F	99.7	300×150×3.5-C	125.1
300×150×2-F	37.1	300×150×2-C	61.3
300×150×1.5-F	22.8	300×150×1.5-C	40.9
300×120×8-F	279.7	300×120×8-C	284.4
300×120×4.5-F	144.9	300×120×4.5-C	149.6
300×120×2.5-F	52.5	300×120×2.5-C	72.5
300×120×2-F	35.6	300×120×2-C	51.4
270×120×8-F	235.3	270×120×8-C	239.3
270×120×5-F	140.4	270×120×5-C	145.0
270×120×4-F	106.5	270×120×4-C	112.3
270×120×2.5-F	46.7	270×120×2.5-C	65.4
245×140×10-F	264.2	245×140×10-C	268.3
245×140×4-F	94.0	245×140×4-C	105.3
245×140×3-F	58.0	245×140×3-C	76.1
245×140×1.5-F	18.0	245×140×1.5-C	32.8
240×160×6-F	156.3	240×160×6-C	165.4
240×160×3.5-F	73.4	240×160×3.5-C	92.4

240×160×2.5-F	42.0	240×160×2.5-C	63.7
240×160×1.5-F	18.1	240×160×1.5-C	35.3
200×160×16-F	303.3	200×160×16-C	313.6
200×160×6-F	117.9	200×160×6-C	124.1
200×160×3-F	45.7	200×160×3-C	59.4
200×160×2.5-F	34.4	200×160×2.5-C	48.6
200×160×2-F	24.1	200×160×2-C	38.1
180×120×8-F	121.1	180×120×8-C	123.5
180×120×3.5-F	48.2	180×120×3.5-C	53.4
180×120×2-F	19.7	180×120×2-C	28.9
180×120×1.5-F	12.3	180×120×1.5-C	21.0
180×80×8-F	102.1	180×80×8-C	103.3
180×80×3-F	36.8	180×80×3-C	38.2
180×80×2.5-F	28.9	180×80×2.5-C	31.0
180×80×2-F	20.0	180×80×2-C	24.3
180×80×1.5-F	11.4	180×80×1.5-C	16.9
150×75×8-F	72.9	150×75×8-C	73.9
150×75×4-F	37.8	150×75×4-C	38.7
150×75×2.5-F	21.9	150×75×2.5-C	23.3
150×75×1.5-F	9.2	150×75×1.5-C	13.1
150×60×6-F	51.8	150×60×6-C	52.3
150×60×3-F	25.6	150×60×3-C	26.3
150×60×2.5-F	20.7	150×60×2.5-C	21.2
150×60×1.5-F	9.5	150×60×1.5-C	12.1
140×80×8-F	66.8	140×80×8-C	68.0
140×80×4-F	34.5	140×80×4-C	35.5
140×80×2-F	14.3	140×80×2-C	16.9

Table 5. Summary of moment capacities of beam specimens in parametric study

Number of Test:10	FE:198	$\frac{M_u}{M_{DSM}}$	$\frac{M_u}{M_{DSM,IR}}$	$\frac{M_u}{M_{CSM,RHS}}$	$\frac{M_u}{M_{CSM,CHS}}$	$\frac{M_u}{M_{CSM}^*}$	$\frac{M_u}{M_{DSM}^*}$
Positive: 104	Mean	1.47	1.18	1.09	1.37	1.04	1.05
	COV	0.142	0.079	0.101	0.108	0.106	0.060
Negative: 104	Mean	1.39	1.23	1.21	1.32	1.09	1.05
	COV	0.182	0.077	0.081	0.194	0.080	0.077
ALL: 208	Mean	1.43	1.20	1.15	1.34	**1.07**	**1.05**
	COV	0.164	0.080	0.103	0.156	**0.096**	**0.069**
	ϕ	0.90	0.90	1.00	1.00	**0.90**	**0.90**
	β	3.38	3.21	2.37	2.70	**2.51**	**2.70**

* Proposed design methods

Table 6. Comparison of SOHS beam test and FE results with predicted strengths